Available online at www.sciencedirect.com
ScienceDirect
Nuclear Instruments and Methods in Physics Research B 260 (2007) 28–33
NIM B
Beam Interactions with Materials & Atoms
www.elsevier.com/locate/nimb

Exploratory nuclear microprobe data visualisation using 3- and 4-dimensional biological volume rendering tools

Harry J. Whitlow [a,*], Minqin Ren [b], Jeroen A. van Kan [b], Frank Watt [b], Dan White [c]

[a] Department of Physics, University of Jyväskylä, PO Box 35 (YFL), FIN-40014, Finland
[b] Centre for Ion Beam Applications, National University of Singapore, Singapore
[c] Department of Biological and Environmental Sciences and the Nanoscience Centre, University of Jyväskylä, Jyväskylä, Finland

Available online 4 April 2007

Abstract

The emergence of Confocal Microscopy (CM) and Atomic Force Microscopy (AFM) as everyday tools in cellular level biology has stimulated development of 3D data visualisation software. Conventional 2-dimensional images of cell (optical) sections obtained in a transmission electron or optical microscopes and more sophisticated multidimensional imaging methods require processing software capable of 3D rendering and mathematically transforming data in 3-, 4-, or more dimensions. The richness of data obtained from the different nuclear microscopy imaging techniques and often parallel information channels (X-ray, secondary electron, Scanning Transmission Ion Microscopy) is often not obvious because subtleties and interrelations in the data could not be rendered in a human interpretable way.

In this exploratory study we have applied the BioImageXD software, originally developed for rendering of multidimensional CM data, to some different nuclear microscopy data. Cells-on-Silicon STIM data from a human breast cancer cell line and elemental maps from lesions on rabbit aorta have been visualised. Mathematical filtering and averaging combined with hardware accelerated 3D rendering enabled dramatically clear visualisation of inter-cellular regions comprising extra cellular matrix proteins that were otherwise difficult to visualise, and also sub cellular structures. For elemental mapping, the use of filtered correlation surfaces and colour channels clearly revealed the interrelations in the data structures that are not easily discernible in the PIXE elemental maps.
© 2007 Elsevier B.V. All rights reserved.

PACS: 68.37.−d; 87.59.−e; 07.78.+s; 42.30.Va

Keywords: Nanobeam; Bio-imaging; Microbeam; PIXE; STIM; Volume rendering; Cells; Organelles

1. Introduction

Confocal Microscopy (CM) combines the foundations of optical microscopy as laid out in Hooke's *Micrographica* from 1665 [1,2] with removal of out of focus laser light by pinhole optics [3,4]. CM is a modern development that in very few years has become a standard tool in cell biology, e.g. [5]. Together with modern image processing techniques it can produce true 3-dimensional images of 3-dimensional objects such as living cells and the surface topography of engineering materials [7]. Parallel with this, Atomic Force Microscopy (AFM) has evolved as a microscopic bio-imaging tool for quantitative mapping of parameters such as topography and elasticity. The need to handle time evolution and multiple CM or AFM image channels such as different fluorescence/excitation wavelength channels and or topography and elastic displacement, has prompted the development of bio-imaging software for combining, filtering and rendering image data in four-, or more dimensional hyperspace in a human-comprehensible manner.

Microscopy with a nuclear microprobe presents similar visualisation requirements to AFM and CM. Conventionally, data have been presented as Particle Induced X-ray Emission (PIXE) and Particle Induced Gamma Emission (PIGE) elemental maps. Identification of the spatial

* Corresponding author. Tel.: +358 14 260 2465; fax: +358 14 260 2351.
E-mail address: Harry_J.Whitlow@phys.jyu.fi (H.J. Whitlow).

0168-583X/$ - see front matter © 2007 Elsevier B.V. All rights reserved.
doi:10.1016/j.nimb.2007.01.316

correlation of two elements, or absence of this, is often difficult to identify in separate, or side by side, images. Colocalisation procedures based on taking the different ratio elemental maps on a pixel to pixel basis is of limited use when the concentrations of trace elements are close to the minimum detection limits. This is because the large statistical fluctuations give rise to large pixel to pixel fluctuations in the ratio map, or division by zero. To take full advantage subtle changes in elemental concentration correlations as well as the energy loss information in Rutherford Backscattering Spectrometry (RBS), Elastic Recoil Detection Analysis (ERDA) as well as on- and off-axis Scanning Transmission Ion Microscopy (STIM) image data, requires the use of image rendering techniques capable of rendering 3- and 4-dimensional data.

Analysis of list-mode mode data comprising a number of parameters written in sequential records is done by histograming. For n parameters, $(n+1)$-dimensions are required to represent the histogram. Conversely, summation over m-dimensions in hyperspace reduces the number of dimensions to $(n-m)$. Histograms with $n \leqslant 2$ can be rendered in terms of physical displacements on a 2D surface as lines, maps or isometric surface plots. In the classification of scales of measurement by the Havard psychologist Stevens [8], the physical displacements correspond to (quantitative) *ratio scales*. Visualisation schemes for histograms with $n \geqslant 3$ requires the use of graphical *sensation scales* based on (qualitative) perception of luminosity, colour and transparency. It is important to bear in mind that unlike ratio-scales, perception of sensation scales, such as a grey-scale, not only varies from person to person but also exhibits a non-linear perception of the sensation. This can be described for a population by Stevens' well known physcophysical law, $\Psi = \phi^{\beta}$ [9,10]. Here, ϕ denotes the stimulus, Ψ the perceived stimulus, and β characterises modality of the stimulus where, e.g. $n = 1.2$ for a grey-scale.

Previously, multidimensional data visualisation has required a top-end workstations because of the need to handle large multidimensional arrays and 3D graphics. The progressive development of computing power and in particular graphics processors has brought this task within the capabilities of a modern personal computers. Today a number of multidimensional visualisation software tools are readily available in the commercial and public domain. Examples are; Paraview [11], Imaris [12] and ImageJ [13,14] which are flexible general multi-purpose tools as well as Osirix [15], Slicer3D [16] and AMIRA [17] which are directed towards rendering X-ray and magnetic resonance tomographic images. In this work we have explored the applicability of software for multidimensional biological image analysis, processing and multidimensional rendering, for visualisation in nuclear microscopy. The particular microscopy image rendering software packages used (ImageJ [13,14] and BioImageXD [18]) were chosen because they are available in the public domain for a wide range of common computer platforms.

2. Colocalisation of PIXE elemental maps

In nuclear microscopy the spatial correlation between the concentration of different elements is generally the subject of study. Colocalisation of regions with particular elemental correlations is often difficult to observe from separate elemental maps, especially if three or more elements are involved.

The ability of the eye to perceive, for instance, red and green light coming from the same point as the colour yellow allows us to readily recognise areas of colocalisation visually in a qualitative manner, even when statistical noise is high. Fig. 1 presents composite colour images of a lesion on a rabbit aorta [19] obtained using the ImageJ programe [13,14]. In the upper image the red, green and blue channels correspond to Cu, Fe and Zn, respectively. These transition

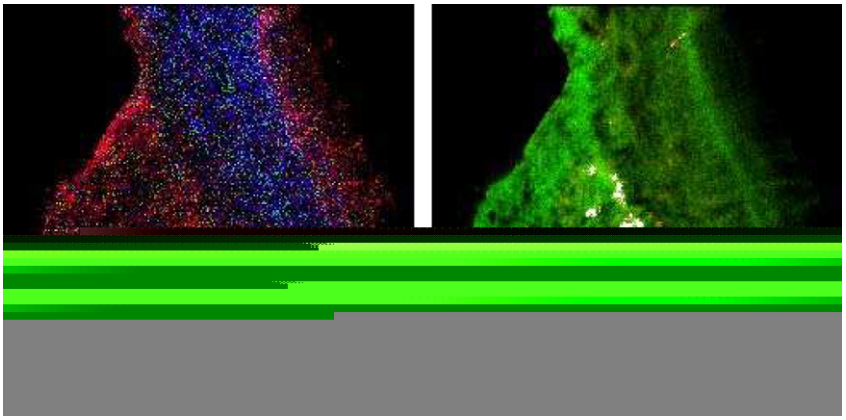

Fig. 1. Colocalisation of PIXE maps using ImageJ [13,14] from PIXE elemental maps of a rabbit aorta arch after [19]. The field size is 1200×1200 μm and the luminosity of each colour channel has been expanded to optimise the visibility of correlations. This destroys the concentration calibrations but inspection of the figure shows it does not affect the clear separation of the signal from the background in the PIXE maps. (Left) The red, green blue channels correspond to Fe, Cu and Zn. (Right) Colocalisation of Ca and P. The white corresponds to colocalised Ca and P while the red and green channels correspond to uncolocalised Ca and P, respectively. The Ca and P were considered to be colocalised when the yield both Ca and P exceeded 50% of the maximum. (For interpretation of the references to colour in this figure legend, the reader is referred to the web version of this article.)

metals are incorporated in proteins that perform catalysis in different sub-cellular organelles such as lysosomes and mitochondria, and in structural and regulatory proteins such as zinc finger gene regulators which bind DNA in the nucleus. Different cell types might tend to have different metal contents due to their differing metabolism, allowing their discrimination on PIXE maps. Colocalisation can be done more quantitatively. For two elements, denoted by red (R) and green (G) whose relative intensities in the R and G channels is, $I_R = C + R_R$; and $I_G = \alpha C + R_G$, respectively. Here C is the colocalisation intensity component, α a relative calibration constant (X-ray fluorescence cross-sections etc.) and R_R and R_G the random intensity components, respectively. Then voxels with a high degree of colocalisation will lie near a straight line, $I_G = \alpha I_R + b$ on an I_G versus I_R scatterplot. Colocalisation of the Ca and P signals for the same data set is shown in Fig. 1. The white colour channel denotes areas where the Ca and P is strongly colocalised that could be indicative of calcium phosphate deposits [19]. While this technique can be set to only render colocalised elements where the elemental composition ratio corresponds to particular chemical compounds it cannot uniquely identify these phases because the use of characteristic X-rays that implies it is totally insensitive to chemical structure. The red and green signals denote non-colocalised Ca and P, respectively. Statistical colocalisation parameters for Fig. 1(b) were 0.37 for Pearson's r_p [20] with $k = 0.93$ and $k = 1.02$ [21] indicating significant colocalisation of Ca and P.

3. 3D surface and volume rendering of STIM data

List mode data from STIM measurements are more challenging because the data are distributed over 5-dimensions (x, y, ΔE, fluence and yield). Fig. 2 compares the same set of COSI-STIM data (a human breast cancer cell grown from the MCF7 cell-line [6,22] imaged using 1 MeV He^+) that has been 3D rendered in different ways using BioImageXD [18]. Here the raw list mode data were sorted into (x, y, ΔE) voxels and in doing so a linear correction [23] to ΔE was applied for the change in pulse height associated with the radiation damage [6] in each pixel [24] of the detector. The resulting 3D histogram was imported to BioImageXD as a stack of grey-scale bitmaps. In order to reduce the effects of the poor counting statistics, the data were mapped to span 16 voxels in the z (ΔE) direction. The simplest presentation is simply a side-by-side grey-scale plot of the stack along ΔE, or alternatively x–y–ΔE sections. Fig. 2(a) is a grey-scale representation of the mean energy-loss. Evidently the organelles in each of the cells can be distinguished. Fig. 2(b) is a free vision parallel stereo pair[1] of the warp-scalar representation of the same data where the grey-scale value in Fig. 2(a) is multiplied by a fixed variable and used to warp a polygon mesh into a 3D surface. Comparing Fig. 2(a) and (b), it is striking that the 3D isometric representation together with colour renders the small small ΔE details such as the short dendrite more prominently and also the sharp peaks in the nucleus are also more clearly discerned. The difficulty in discerning the details of the dark grey dendrite from the background in Fig. 2(a) is a consequence of Stevens' law [10] (above) which implies that the change is perceived intensity is greatest for lighter parts of the image than darker which was confirmed by comparing with a negative image where the dendrite details are more clearly distinguishable. A further observation is that the image is apparently noisy. However, close inspection reveals the noise is confined to the regions covered by the cells, or extracellular proteins. In this case the intensity averaging effect of the eye–brain system makes the noise seen in Fig. 2(b) less discernible in the grey-scale image Fig. 2(a).

Fig. 2(c) presents a 4-dimensional representation of the energy loss distribution for the same data set. By assigning these levels different colours and observing the image during slow rotation to enhance the sensation of vertical depth in the image, it was found the "noise" was in fact some structure in the energy loss distributions along the z direction. Such structure is destroyed in calculation of the average energy loss for the representations, (Fig. 2(a) and (b)). This can also be seen, although not as easily discerned, in the stereo image, Fig. 2(c). Here the data are smoother, but within the cell from one (x,y) pixel to the another, the modal energy loss and straggling varies considerably. In contrast, outside the cell the modal energy loss and straggling exhibit stopping media, and hence the stopping force, is inhomogeneous within the beam spot. This situation even give rise to multi-modal energy-loss distributions as was the case in our previous polka-dot stopping measurements [26,25].

The clear structure in Fig. 2 clearly shows the organelles in the cell. The nucleus can be clearly discerned as a region of high ΔE surrounded by a thin narrow region with low ΔE delineating the nuclear envelope. The large ΔE for the nucleus is probably associated with the densely packed chromatin within the nucleus. The three large ΔE peaks in the nuclear region correspond to dense regions that are very likely to be nucleoli, (sites of ribosomal rRNA transcription and ribosomal assembly) which have previously been described to be electron dense [27,28], possibly by accumulation of high levels of metal ions [28–33], such as Zn [32], probably in proteins such as zinc-finger gene-regulators. While these peaks could be associated with dense thicker regions in the cells after drying they are most likely to be nucleoi because optical microscope images of the carcoma cells revealed the nuclei contained 2–5 nuceloli with similar lateral size to the peaks in (Fig. 2). The ΔE peaks outside the nuclear region of the cell can be associated with organelles like the Golgi apparatus, lysosomes, peroxisomes, mitocondria. These structures are mainly proteins,

[1] To view free vision parallel (wall-eye) stereo images: (i) Place the images in the centre of your field of view, (ii) slowly cross you eyes so that a third 3D image appears between the other images and (iii) focus on the middle image so it becomes sharp.

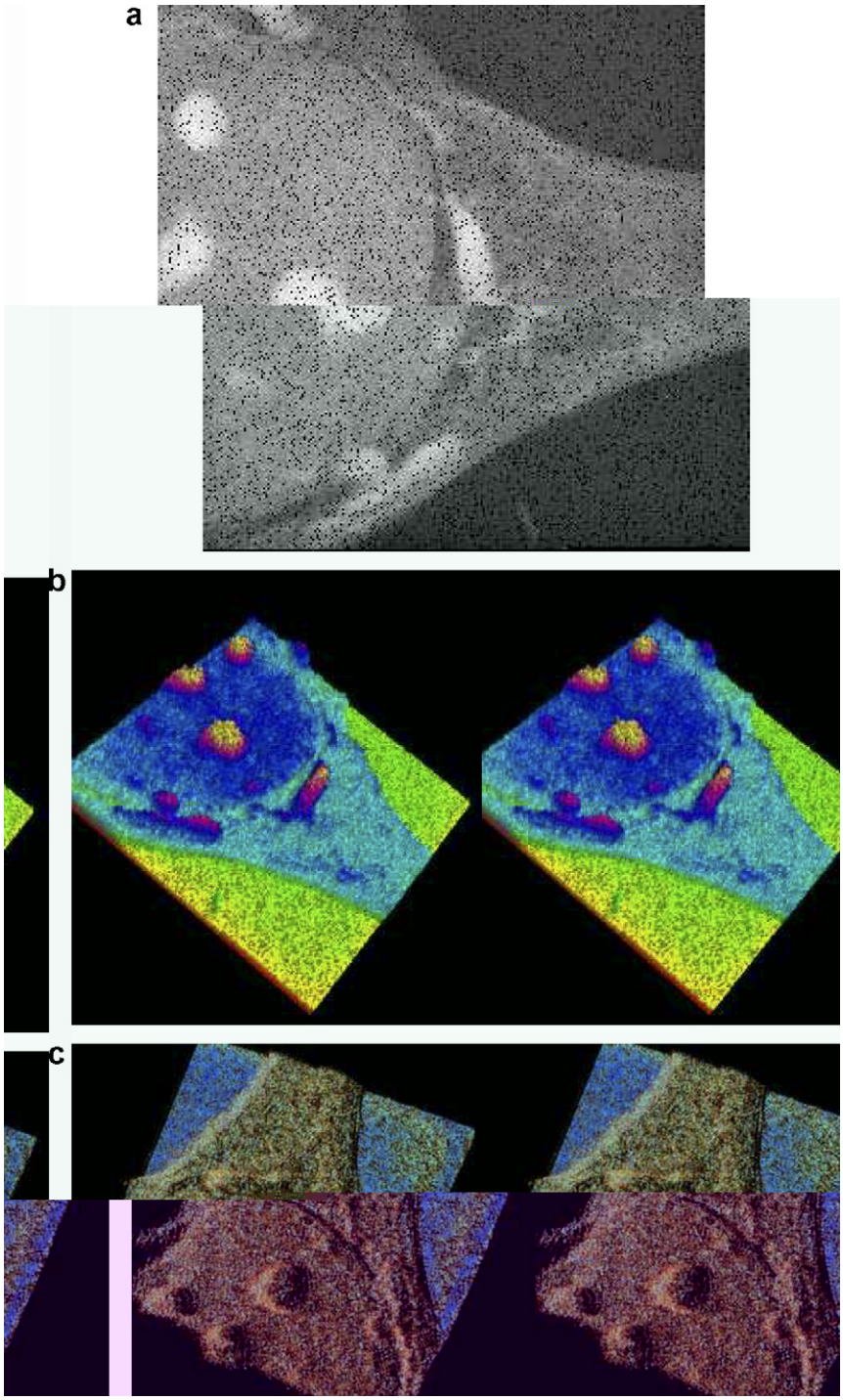

Fig. 2. Volume rendering of COSI–STIM data for a human breast cancer cell After [6]. The width of the field is 15 μm. (a) Grey-scale map of the average energy loss. White corresponds to maximum energy loss. (b) Free vision parallel stereo pair of Warp-scalar representation the average energy loss map using BioImageXD with smoothing. (c) Free vision parallel stereo pair representation of the data represented by (x, y, z, colour + luminance) where z corresponds to ΔE, and colour + luminance corresponds to yield. Increasing yields correspond to the colour sequence red through green to blue. (For interpretation of the references in colour in this figure legend, the reader is referred to the web version of this article.)

often containing transition metals such as Cu, Zn, Fe, Mn and Co. Cytoskeleton components such as actin fibres are dense protein structures, which appear to be visible here despite lack of abundant transition metal content. Moreover, these organelles have internal structures on a scale of 1–100 nm that would give rise to the wide inter-pixel variations in energy loss and straggling seem in Fig. 2.

Fig. 3 shows a warp-scalar of a COSI–STIM image of a cohort of breast cancer cells. In the grey-scale map of mean energy loss, some structure between the cells with small ΔE